**PAPER** • **OPEN ACCESS**

# Flow cytometry as an analytical method of drug-induced apoptosis in 3D bioprinted melanoma cells

To cite this article: Maryke de Villiers and Lissinda H Du Plessis 2023 *Biomed. Mater.* **18** 045031

Biomedical Materials

PAPER

# Flow cytometry as an analytical method of drug-induced apoptosis in 3D bioprinted melanoma cells

**Maryke de Villiers and Lissinda H Du Plessis***

Centre of Excellence for Pharmaceutical Sciences, Faculty of Health Sciences North-West University, Private Bag X6001, Potchefstroom 2520, South Africa

* Author to whom any correspondence should be addressed.

**E-mail:** Lissinda.DuPlessis@nwu.ac.za

**Keywords:** 3D bioprinting, apoptosis, etoposide, extrusion-based bioprinting, flow cytometry, gelatine/alginate hydrogel, melanoma

Supplementary material for this article is available online

OPEN ACCESS

RECEIVED
21 February 2023

REVISED
12 May 2023

ACCEPTED FOR PUBLICATION
23 June 2023

PUBLISHED
3 July 2023



## Abstract

Three-dimensional (3D) cell culture systems have gained increasing interest in drug discovery and tissue engineering due to its inherent advantages in providing more physiologically relevant information and more predictive data for *in vivo* tests. Along with the development of more physiologically relevant 3D cell culture models, researchers bear the responsibility to validate new cell assay techniques capable of measuring and evaluating constructs that are physically larger and more complex compared to two-dimensional cell cultures. It is important to note that assays based on monolayer cultures may be insufficient for the use in 3D cell cultures models. In this study we firstly fabricated a 3D bioprinted hydrogel melanoma scaffold. This was used to validate a flow cytometry-based analytical method as a tool for 3D bioprinted structures to assess drug-induced apoptosis. The results indicated high robustness, reproducibility and sensitivity of the flow cytometric method established on the 3D cell-laden A375 melanoma hydrogel scaffolds. Over and above this, it was possible to determine the effect of etoposide on A375 melanoma cells using Annexin V and propidium iodide apoptosis assay.

## Abbreviations

| | |
|---|---|
| $CaCl_2$ | Calcium chloride |
| CAD | Computer-aided design |
| CV | Coefficient of variation |
| DMEM | Dulbecco's modified eagle medium |
| FBS | Foetal bovine serum |
| FITC | Fluorescein isothiocyanate |
| FSC | Forward scatter |
| LOD | Limit of detection |
| LOB | Limit of blank |
| LLOQ | Lower limit of quantification |
| MFI | Mean fluorescence intensity |
| PBS | Phosphate buffered saline |
| PE | Phycoerythrin |
| PI | Propidium iodide |
| SD | Standard deviation |
| SSC | Side scatter |

## 1. Introduction

Cell-based assays are a crucial element of the drug discovery process and pharmaceutical development. Assays using cultured cells are simple, fast, and cost-effective, versatile and easily reproducible as well as being the first step before *in vivo* tests can be considered. For decades, cell biology research has depended on two-dimensional (2D) cell culture methods in which simplified monolayers of cells are produced on rigid, flat surfaces [1–3]. These cell cultures are simple to handle, image, and analyse using standard laboratory equipment. Monolayer 2D cell cultures lack biological and mechanical indicators that would normally be experienced *in vivo* [4]. The absence of molecular and cellular interactions in

2D cell models prevents our understanding of cell-to-cell and cell-to-extracellular matrix (ECM) interactions, hence restricting their relevance to cancer biology. Furthermore, the inability of ECM to support and interact with the various cells may decrease the biological applicability of these 2D cell culture systems [5]. Due to the limitations of these 2D models in simulating functional live tissue, data regarding *in vivo* reactions has frequently been deceptive and non-predictive. It has been proven that three-dimensional (3D) cell cultures hold the potential to overcome some of these limitations by mimicking the natural microenvironments of cells in tissue more accurately. Cells cultured in a 3D environment are exposed to spatiotemporal cues such as cell-to-cell and cell-to-ECM interactions, which influence signal transduction, gene expression, and cellular behaviour during proliferation and differentiation [1–3]. As a result, a large amount of effort has gone into developing 3D cell culture techniques and materials that can replicate tissue-specific features and evaluate drug responses more accurately [6, 7]. Along with the development of more physiologically relevant 3D cell culture models, researchers bear the responsibility of validating new cell assay techniques capable of measuring and evaluating constructs that are physically larger and more complex compared to 2D cell cultures [8].

3D bioprinting is a progressive biomanufacturing technology that enables the simultaneous deposition of living cells and diverse biomaterials utilising CAD to generate tissue-relevant 3D constructions with specific structural architectures [9, 10]. In recent years, 3D bioprinting has made considerable technical advances, along with multiple types of bioprinters with varying materials, speeds, and accuracies, making it the most promising technology for manufacturing 3D models which could be utilised for cancer biology and screening of anticancer drugs [11]. The different types of bioprinting technologies include extrusion-based bioprinting, laser-based and laser-assisted bioprinting and inkjet-based bioprinting [12]. Extrusion-based bioprinting has recently become the most widespread bioprinting technique utilised for 3D cell culture due to its low cost, adaptability, and scalability [6, 13–16]. In extrusion-based bioprinting, the printer is generally composed of a temperature- and pressure-controlled reservoir as well as a dispensing system that extrudes unbroken filaments of biomaterials through a pneumatic, piston-driven, or screw-driven system [6]. Extrusion-based bioprinters can print biomaterials with a wide range of viscosities and high cell densities; however, cell viability can possibly be compromised owing to the high pressures encountered during printing [17, 18]. 3D bioprinting requires the use of biomaterials as bioinks, these bioinks can be established from a range of natural and synthetic biomaterials or combinations thereof. Often, it is required to adjust the biomaterial formulation for a specific application in order to enhance the biological and/or physicochemical properties of the bioink intended to be used [19, 20]. Water dispersible polymers, otherwise identified as hydrogels are favourable due to their chemical structure and promising environment for cell development. Due to the hydrogel's high capacity for water retention, they are classified as biocompatible materials that promote cell-friendly environments [21, 22]. Natural hydrogels offer more biocompatibility, but synthetic hydrogels are usually more affordable, simpler to manipulate, and more homogeneous from batch to batch [23, 24]. Hydrogels perform a notably vital role as they are penetrable to nutrients, oxygen, and other soluble compounds in the surrounding medium, which leads to higher cell viability. Typically, natural hydrogels, such as chitosan, collagen, hyaluronic acid, and alginate, are used in 3D bioprinting applications to improve biocompatibility [25]. The key to the effectiveness of 3D bioprinting is the capacity of the bioink to develop strong, high-resolution constructs without affecting cell viability during and after the printing process. Hence, material selection and printing parameter optimisation can have a significant impact on the bioink's characteristics, which have to be integrated in order to print tissue-relevant, biocompatible, and functional structures [26]. Alginate and gelatin combination hydrogels are among the most commonly used and well-characterised biomaterials for 3D cell culturing owing to their many desired properties, including non-Newtonian rheology, strong biological compatibility, degradation, cell encapsulation abilities, and overall good printability [27]. A range of printing parameters can determine the printability of scaffolds. The shear-thinning, biomechanical and biochemical characteristics of bioinks are determining factors for successful bioprints. Printing accuracy can provide answers to the macroscopic mechanical properties of the hydrogel materials, including the stiffness and the ability of the printed construct to support itself. Microscopically hydrogel porosity is related to water uptake and swelling, as well as degradation kinetics. Important factors to determine as cells needs more space as they progressively form new tissue [19, 20, 23].

There are currently a vast number of techniques for generating 3D cell culture models, each of which renders spheroids or scaffolds of varying size, form, and complexity. This complicates the standardisation of 3D cell culture analytical techniques and data generation [28]. Most existing analytic methods were developed primarily to fulfil the needs of 2D cell cultures and have not yet been fully adapted toward 3D cell culture platforms [29]. With the advances made

in creating 3D cell models, it is becoming more critical that the models developed using these approaches be compatible with relevant analytical methods that allow the extraction of useful biological data from drug-screening research [30]. When employing 3D models for drug screening applications, it is also important to address the accuracy and precision in which the data is collected and how the result of the screening is being interpreted [31]. For effective data collection and analysis of 3D cultures, it is necessary to overcome the underlying challenges posed by the considerably more complex nature of 3D cell models compared to 2D cell models [32]. Some limitations of current 3D culture cell-based assays include optical light scattering, light absorption and poor light penetration with prolonged imaging acquisition times, and imaging of multicellular cultures and cells grown within complex geometrical structures, and as a result limiting the applications of 3D cultures in high-content screening [33]. The natural distribution of cells throughout the 3D environment, as well as changes within the population of encapsulated 3D cell models, demand a thorough data-collecting strategy to obtain the necessary information. Furthermore, in 3D cell models embedded within a hydrogel environment, the hydrogel itself may interfere with or affect assay readouts or imaging techniques [31, 34]. Therefore, standardising, and validating 3D cell culture model assay approaches to provide reproducibility, automation, and high throughput analysis is much needed for further advancements in 3D cell culture models [28]. The implementation of high-content imaging assays on typical 3D cell culture models presents numerous obstacles. For example, the quantitative assessment of 3D cells in a 96-well plate is variable and unreproducible owing to the challenges in the manual handling of the hydrogel constructs and the supporting medium [35]. In addition, imaging and image processing present with complications since the cells cultured in 3D models are not in individual focal planes. While such factors may not be recognisable in traditional 2D cell culture screenings, they can become significant sources of irregularity in 3D cell culture high-content imaging assays. Furthermore, the majority of hydrogel scaffolds are opaque and inadequate for imaging. Imaging techniques are a crucial factor in determining the overall outcome of an experiment [33].

Flow cytometric analysis is a technique that can be considered for cell analysis in 3D cell culture models that requires an adjusted strategy. For flow cytometry analysis, cells must be completely isolated in a single fluid solution. This signifies that the hydrogel construct is not suitable for use in its solid condition and must be de-gelated before analysis [34, 36]. In various biological applications, flow cytometry is regarded as the gold standard for high-throughput single-cell characterisation assays. Traditional cancer cell analysis assays often only consider the average response of a group of cells, which may result in inaccurate findings and the loss of important data, while single-cell analysis can evaluate cell-to-cell changes in a large and heterogeneous cell population [37]. Flow cytometry, laser scanning cytometry, and automated microscopy are a few examples of traditional single-cell analysis methods. For decades, these approaches have been employed to investigate cellular heterogeneity. Flow cytometry has previously shown to be a powerful instrument in the development of cell treatment processes, implying that it may be a critical component in the field of 3D bioprinting processes, since it is high-throughput screening compatible and varied in terms of measurable cell properties [34, 38]. Flow cytometry allows for analysis of multi-parametric parameters simultaneously and can provide quantitative and rich cellular information regarding cell death. Moreover, flow cytometers hold the potential of quantifying both necrosis and apoptosis in the same population of cells using different dyes and antibodies [39]. Researchers also recommend using flow cytometry and microscopy as complementary technologies, seeing as how their combination provides new opportunities for the development of relevant and reliable quantitative cell-based assays. Flow cytometry and microscopy can both be used individually or in combination [40]. However, it is essential that one should not simply accept that assays developed for monolayer cultures would be adequate for use in 3D cell cultures as some adjustments will be needed [8, 34].

Many types of flow cytometric techniques can be used in drug effectiveness testing [41]. By combining Annexin V as a FITC with PI as an exclusion marker for cell viability, this technique can concurrently distinguish between apoptosis and necrosis and identify apoptotic cells [42, 43]. The Annexin V signal is an extremely sensitive approach for identifying cell death, where PI is used to identify necrotic or late apoptotic cells, which are characterised by the loss of plasma and nuclear membrane stability. Flow cytometry data are shown as 2D dot plots in which PI is displayed against Annexin V-FITC. These plots can be divided into four quadrants: viable cells which are negative to both probes; apoptotic cells which are PI negative and Annexin positive; late apoptotic cells which are PI and Annexin positive; and lastly necrotic cells which are PI positive and Annexin negative [43]. Cells have significant levels of autofluorescence that are detected by highly sensitive flow cytometers. Background noise is subtracted from the total signal emitted by the cell population in the data analysis phase [44]. It has been proven that commercial biomaterial ink containing nano-cellulose interfered

with flow cytometry proliferation analysis, causing significant scatter and fluorescence background. This necessitated a data deconvolution step [34]. Data deconvolution can prove challenging, especially if heterogeneous cell samples will be used, as applying the same statistical or mathematical model to different cell types or markers is not feasible [45].

In this study, the validation of a flow cytometry analysis method to analyse drug-induced apoptosis in 3D bioprinted melanoma cells is reported. The first aim of the study was to formulate and quantitatively characterise an alginate–gelatine biomaterial ink, and to optimise the extrusion-based bioprinting parameters needed to guarantee desired tissue functions and cellular activity and to realise high cell viability of a printed melanoma scaffold. The strategy includes A375 melanoma cells 3D bioprinted in an alginate–gelatine hydrogel scaffold. The second aim was to validate the Annexin V/PI flow cytometric apoptosis method in the 3D bioprinted hydrogel scaffold, where the first step was to optimise the de-gelation and fluorescent staining. It was important to determine if the hydrogel material interfered with the scatter profile or Annexin V/PI fluorescence and if data deconvolution was needed. Specificity, precision, and sensitivity of the methods were determined. Additionally, to assess apoptosis in the 3D bioprinted A375 melanoma cell scaffolds, a well-recognised anti-cancer drug etoposide, known to induce apoptosis, was used to treat melanoma cells, and compared to a fluorometric mitochondrial activity assay the resazurin assay to assess how the validated method compared to other methods.

## 2. Materials and methods

### 2.1. Materials

Alginic acid sodium salt (powder, 180947) with a viscosity of 15–25 cP, 1% $H_2O$, a molecular weight of 120 000–190 000 g $mol^{-1}$, and a mannuronic acid to guluronic acid (M/G ratio) of 1.56), were purchased from Sigma-Aldrich (Merck, Darmstadt, Germany). The gelatine from bovine skin Type B (granules, gel strength 50–120, G6650) and PBS (powder, P3813), were also purchased from Sigma-Aldrich (Merck, Darmstadt, Germany). The 3 ml pneumatic syringe/cartridges and 22, 25 and 27G high-precision conical bioprinting nozzles were purchased from Cellink® (Gothenburg, Sweden). The cross-linking solution ($CaCl_2$) for alginate was purchased from Cellink® (CellINK AB, Gothenburg, Sweden) and stored at room temperature and utilised after bioprinting of the scaffold. The A375 cell line (Catalogue no. CRI-1619) was purchased from the American Type Culture Collection (ATCC, Manassas, VA, USA). The cell culture medium consisted of high glucose (DMEM/High-glucose, HyClone, Separations, Johannesburg, South Africa) that contained 4500 mg $l^{-1}$ glucose, 4 mM L-glutamine and 1 mM sodium pyruvate. The medium was supplemented with 10% FBS, (ThermoFisher Scientific, Johannesburg, South Africa), 1% penicillin/streptomycin (10 000 U $ml^{-1}$) 1% non-essential amino acids (Lonza, Whitehead Scientific (Pty) Ltd, Cape Town South Africa). The de-gelating solution consisted of 4% (w/v) trisodium citrate (Sigma Aldrich, Merck, Darmstadt, Germany). For cell the viability assays Trypan blue solution and commercial resazurin kit were purchased from Sigma-Aldrich®, Merck (Pty) Ltd (Darmstadt, Germany). Alexa Fluor® 488 Annexin V and PI kit purchased from BD biosciences (Franklin Lakes, New Jersey, U.S) was used. Etoposide (powder, 98.0%–105.0% E1383-25MG) purchased from Sigma-Aldrich (Merck, Darmstadt, Germany) was used to induce apoptosis.

### 2.2. Cell culturing

In this study, A375 (ATCC® number CRl-1619™) melanoma cancer cells were used in the 3D bioprinted scaffold. Dulbecco's Modified Eagle's Medium–high glucose (DMEM), supplemented with 1% non-essential amino acids, 1% L-glutamine, 1% penicillin and 10% FBS, trypsin 0.25% Ethylenediaminetetraacetic acid (EDTA) , and sterile PBS solution were used. Briefly, A375 cells were cultured in a 75 $cm^2$ flask with 15 ml of DMEM media and were incubated in a humidified incubator maintained at 37 °C with 5% $CO_2$ until 80%–90% confluency was reached when cells then were split and passaged to ensure cell stability. To assess routine cell viability cells were counted microscopically with Trypan blue exclusion as previously described [46].

### 2.3. Formulation of hydrogel biomaterial ink

Six different alginate and gelatine blends were investigated as possible bioinks with alginate and gelatine in different weight ratios: alginate 7% + gelatine 8% (w/v) (A7G8), alginate 6% + gelatine 8% (w/v) (A6G8), alginate 5% + gelatine 8% (w/v) (A5G8), alginate 7% + gelatine 5% (w/v) (A7G5), alginate 2% + gelatine 8% (w/v) (A2G8), alginate 2% + gelatine 5% (w/v) (A2G5). The hydrogel blend was prepared using a combination of methods previously described by Chung *et al* [47] and Duan *et al* [48]. Gelatine granules were dissolved in 100 ml PBS, at 60 °C for 1 h with a magnetic stirrer until a thick solution was formed. The alginate powder was gradually added to the gelatine solution and mixed for 30 min with a magnetic stirrer until a thick solution is formed. A Pro Scientific Homogenizer mixer was used to guarantee a homogenous mix of the two materials and to remove trapped air bubbles. Gels had to be viscous enough to maintain a shape, but still free flowing to be filled in cartridges. Each cartridge was

filled up to 2 ml for individual tests. The 25G sterile high-precision nozzle (Cellink, Sweden) was fixed to 3 ml plastic cartridges. The hydrogel was then sterilised via short-cycle autoclaving and stored at 37 °C to prevent gelatine sol–gel transition.

### 2.4. Printability of hydrogel biomaterial ink

#### *2.4.1. Strand width tests*

The strand width tests of the various alginate–gelatine hydrogels were determined by using a single-strand extrusion test, adapted from Di Giuseppe *et al* [49]. Firstly, a single layer, continuous strand of the hydrogels using a 27G and 25G sterile high precision nozzle (Cellink, Sweden) following a path designed using Fusion 360 CAD software was printed. A single strand of 23.80 mm in length and 0.3 mm in diameter was printed (supplementary material, figure S1). This strand-thickness of the design represents the actual nozzle diameter. Due to the pooling of the viscous gel, the strand width was greater than the internal diameter of the needle tip. Each strand's width and diameter were measured using digital callipers (grip, 0–150 mm). The strand was measured at multiple locations and averaged. Photographs were taken after each line test. Image dimensions were employed to establish a scale to quantify strand width and diameter with ImageJ software. The repeatability of the single-line print was determined by comparing strand width and photographs of printed lines on ten separate prints. Red food colouring (1 drop) was added to the hydrogel mix to aid in the visualisation of printed lines.

Different print parameters were investigated including printing speeds of 4, 6, 8, 10 and 12 mm $s^{-1}$, extrusion pressures of 40, 50, 70 and 100 kPa were evaluated at a constant temperature of 37 °C (per manufacturer's instructions) to optimise printability and parameters of the hydrogels, bearing in mind that minimizing the pneumatic pressure and speed of the printing nozzle can result in higher cell viabilities [50]. Printability tests were conducted using glass microscope slides as the printing surface.

#### *2.4.2. Parameter optimisation index (POI)*

A POI method is to standardise the optimisation process of bioprinting and to determine the relation between printing variables following a grading system [51]. The method considers the relation between extrusion pressure, material extrusion rate and nozzle diameter and the shear stress exerted onto the material from the nozzle. The method proved accurate for conical print nozzles with a pneumatic-based bioprinter [52]. High POI values indicate that a scaffold can be printed with high accuracy and mechanical strength with lower extrusion pressure and decreased line width [51]. The POI was calculated using the values of the strand width test.

The first equation is used to determine the POI in a series of experiments using the same bio-ink

$$\mathrm{POI} = \frac{1}{t_{\mathrm{line}} \times D_{\mathrm{G}} \times p} \tag{1}$$

The second equation is used to determine the POI of a specific bio-ink across a range of printing parameters and to normalise, relative to the maximum POI in the experimental range

$$\mathrm{POI_i} = \frac{\mathrm{POI_i}}{\mathrm{POI_{max}} \times n} \tag{2}$$

where $t_{\mathrm{line}}$ = printed line width, $D_{\mathrm{G}}$ = needle gauge, $p$ = extrusion pressure,

$\mathrm{POI_i}$ = POI for an individual set of parameter,

$\mathrm{POI_{max}}$ = maximum POI of the range tested and

$n$ = total number of parameter combinations.

#### *2.4.3. Printing accuracy*

The accuracy of the printed strand width was calculated using a formula adapted from Di Giuseppe *et al* [49]. This printed structure was then compared with the designed structure, to obtain a percentage printing accuracy for each sample using the following equation, with the average dimensions of the ten grids printed

$$\text{Printing accuracy } (\%) = \left(1 - \frac{A_i - A}{A}\right) \times 100 \tag{3}$$

where $A_i$ is the designed grid measurement and $A$ is the printed design measurement.

### 2.5. Mechanical traits of the biomaterial ink

#### *2.5.1. Porosity of formulated alginate–gelatine hydrogels*

JTo determine the porosity of the optimised hydrogel, an adaption of the method of Cao *et al* [53] was utilised. Each hydrogel (2 ml) was deposited in a 6 well-plate, cross-linked with 3 ml of a 2% $CaCl_2$ cross-linking solution and then incubated for 5 h at 37 °C. After complete cross-linking, the hydrogel discs were removed and washed with PBS and left to dry for 30 min on a paper towel to drain excess fluid. After 30 min the dry hydrogel disc was weighed. Subsequently the hydrogel discs were suspended into deionised water allowing discs to reabsorb the water and weighed again without drying. Finally, the disc was resuspended into the water and weighed with the hydrogel disc submerged in the water. The porosity (%) of the different hydrogels was calculated using equation (4)

$$\text{Porosity } \% = \frac{M_{\mathrm{Wet}} - M_{\mathrm{dry}}}{M_{\mathrm{Wet}} - M_{\mathrm{sub}}} \tag{4}$$

where $M_{\mathrm{Wet}}$ is the mass of the wet disc taken out of the water;

$M_{dry}$ is the mass of the dry disc; and

$M_{sub}$ is the mass of the disc submerged in deionised water.

*2.5.2. Degradation rate of formulated alginate–gelatine hydrogels*

The method used for determining the degradation rate of the hydrogel was adapted from Aldana *et al* [54]. Degradation tests were conducted over a 1 week period in different solutions, where 2 ml Hydrogel were suspended in a 6-well plate and cross-linked with 3 ml of a 2% $CaCl_2$ (w/v) solution and incubated for 5 h at (37 °C with 5% $CO_2$) to form a disc. After complete cross-linking the formed hydrogel disc was removed and dried for 30 min and weighed (Wd0). The hydrogel discs were then resuspended in 3 ml $dH_2O$ or DMEM media and weighed again after 24 h, 48 h and 168 h (Wd*t*) to establish percentage degradation (*D*) that had taken place. After each weighing, fresh DMEM media and $dH_2O$ were added to the well plates before incubation.

Degradation percentage was calculated using equation (5)

$$D\% = (\mathrm{Wd0} - \mathrm{Wd}t) \times \frac{100}{\mathrm{Wd0}} \quad (5)$$

*2.5.3. Swelling ratio of formulated alginate–gelatine hydrogel*

The method of calculating the swelling ratio was adapted from Chawla *et al* [55]. Scaffolds were printed and cross-linked with 2% $CaCl_2$ (w/v) and after complete cross-linking of scaffolds, they were submerged in deionised water at 37 °C. Once the absorption equilibrium was reached, scaffolds were taken out and weighed, thereafter dried on filter paper for an hour and then weighed again. The swelling ratio was calculated using the following equation (6)

$$\text{Swelling ratio} = \frac{W_1 - W_0}{W_0} \quad (6)$$

where $W_1$ is the weight of the wet scaffold after water absorption and $W_0$ is the weight of the dry scaffold before water absorption.

### 2.6. Bioprinting of A375 melanoma cells

The cells were mixed with the hydrogel before bioprinting. Briefly, hydrogels were heated to 37 °C for 1 h to reduce viscosity, before 2 ml of the hydrogel was transferred into 3 ml cartridges. The A375 melanoma cells were trypsinised and centrifuged and resuspended in 2 ml of DMEM to reach a final cell concentration of $1 \times 10^6$ cells per 100 µl. The 400 µl of DMEM-cell suspension were added to the 2 ml hydrogel to reach a concentration of $4 \times 10^6$ cells per 2 ml hydrogel. As 2 ml hydrogel renders six scaffolds, the approximate concentration of cells per scaffold was $6 \times 10^4$ cells. The cell suspension was manually transferred by pipette into the middle of the hydrogel blend, and manually stirred into the bioink to create an evenly distributed single-cell suspension. A 1:5 ratio of media to hydrogel showed uniform cell distribution and did not affect the hydrogel viscosity or extrudability. Samples were then printed using 27G nozzles with the BioX bioprinter using its in-built cleanroom environment. The print head was heated to 37 °C and the print bed to 10 °C and the scaffolds were printed. Once the scaffolds were printed, the samples were crosslinked with 2 ml (4% w/v) $CaCl_2$ for 10 min. The crosslinked hydrogels were then washed with DMEM to remove excess calcium ions. DMEM media was added to each well and cells included in the 3D printed structures were cultured at 37 °C and 5% $CO_2$.

### 2.7. De-gelation of scaffold

In order to analyse cells, the sample should be suspended in a fluid, usually a buffer, with as little as possible debris, as these can interfere with the analyses. After 48 h of incubation the scaffold was cut into small sections with a scalpel. These sections were incubated in the de-gelating solution, tri-sodium dehydrate 4% (w/v) and sterile filtered water, at a temperature of 37 °C for 30 min. After 30 min the solution was inspected if de-gelated completely. After de-gelation, the cell-suspensions were centrifuged at 3000 rpm for 5 min. The supernatant was removed, and the cell pellet resuspended in DMEM or PBS (depending on the analysis method used).

### 2.8. Cell staining

In this study the measurement of apoptosis and cell viability Alexa Fluor® 488 Annexin V and PI kit purchased from BD biosciences (Franklin Lakes, New Jersey, U.S) by means of flow cytometry was validated. Cells were grown for 48 h in the alginate–gelatine hydrogel (3D bioprinted) and was compared with cells not bioprinted in the hydrogel and suspended in PBS (2D cell cultures). Unstained cells were used as a negative control.

For cells not bioprinted in hydrogel, after cells have been grown for 48 h, cells were washed with PBS twice and then trypsinized and centrifuged at 1750 rpm for 5 min, the supernatant discarded, and cells were resuspended in 500 µl PBS (control group unstained) or 500 µl 1× Annexin binding buffer. The Annexin binding buffer consisted of 0.1 M Hepes (pH 7.4), 1.4 M NaCl, and 25 mM $CaCl_2$. A total volume of 5 µl of fluorochrome-conjugated Annexin V and 5 µl PI was added to the 500 µl cell suspension. The samples were incubated for 10–15 min at 37 °C, in the dark.

For cells grown in the hydrogel scaffold, after 48 h scaffolds were de-gelated. After centrifuging, the supernatant was discarded, and cells resuspended in 500 µl PBS (control group unstained) or 500 µl 1X Annexin binding buffer. A total volume of 5 µl of

fluorochrome-conjugated Annexin V and 5 µl PI was added to the 500 µl cell suspension. The samples were incubated for 10–15 min at 37 °C, in the dark.

### 2.9. Flow cytometric analysis

The flow cytometric analysis was performed using the BD FACSLyric™ flow cytometer equipped with a blue 488 nm laser for excitation of FITC (green) and PI (red). When using the FACSLyric™ flow cytometer a defined sample volume of 500 µl was analysed. At least 10 000 cellular events were analysed for each sample. Gates were applied to these FSC/SSC dot plots to exclude cellular debris, de-gelated hydrogel debris and other background particles. Unstained negative controls, as well as positive controls, were included in all analyses.

### 2.10. Method validation

In this study we followed a quasi-quantitative approach evaluating specificity, precision, and sensitivity to validate our analysis method [56]. Specificity was determined in terms of how well the populations of interest could be separated and distinguished from gel particles. Firstly, the hydrogel was diluted 1:5 (100 µl gel in 400 µl PBS; total sample volume 500 µl) and analysed. This was then compared with the formulated hydrogel that was bioprinted, cross-linked and de-gelated. Calibration beads (size 2–3 µm) were used as additional controls and both beads without any fluorescent marker (unstained beads) and FITC labelled and PI labelled fluorescent beads were bioprinted, cross-linked and de-gelated. In addition, two samples bioprinted in the hydrogel were used, unstained untreated A375 cells, and untreated cells stained with Annexin V and PI. The intra-assay precision was evaluated through analysing the same assay repeated on three separate occasions with all samples. The inter-assay precision was evaluated through analysing the same sample twice (two different runs on the same sample). The precision approval criteria for cell-based assays are 10%–25% CV. Higher imprecision (30%–35% CV) is often acceptable for rare populations. Sensitivity of the assay depends on the type data/output generated but the goal is to minimise false positive or false negative results. In terms of the Annexin-V/PI assay for cells bioprinted in gel, it was important to be able to prove that the gel material (particles) did not interfere with the number of events counted (% cells counted) or the intensity of the fluorescence parameters (geometric mean MFI). Imprecision in the range of 20%–35% CV has been reported to be acceptable for biomarker methods and was used in this study. In terms of the minimum number of events that counted as true events and were not considered background for this study was set at 200 events. For these assays, analytical sensitivity involves the LOD, the ability to distinguish from the background-LOB, and the LLOQ [56].

### 2.11. Anti-cancer activity

Etoposide was prepared in dimethyl sulfoxide (DMSO) as a stock solution of 50 mM. Cells were treated with two concentrations of etoposide, 50 µM and 100 µM, based on half maximal inhibitory concentration ($IC_{50}$) values previously established for A375 cells [57], for 4 h at 37 °C. The final concentration of DMSO in the treatment of cell media was never higher than 1%. Untreated cells served as the control. Cells were de-gelated and stained as previously described.

### 2.12. Resazurin based cell viability assay

In this study the results of etoposide-induced cell viability in the 3D bioprinted hydrogel scaffolds measured by a plate reader resazurin-based assay were compared with the results of the validated flow cytometric analysis method. Resazurin (blue and non-fluorescent) is reduced by dehydrogenase enzymes to generate the red fluorescent dye resorufin, which is maintained in the cytoplasm and mitochondria of living cells. Fluorescence, which is proportional to the number of live cells in the sample, can be used to measure the quantity of resorufin present [58].

Cells of 80%–90% confluency cells were in equal amount in a 96-well plate. A control group media and untreated cells was used to quantify background fluorescence of the de-gelated hydrogel or media. The cells were treated with etoposide 50 µM, 100 µM and incubated for 4 h at 37 °C. Following the manufacturer's instructions, after incubation, resazurin dye solution was added in an amount equal to 10% of the culture medium volume. Cell cultures were returned to the incubator for 2–4 h depending on cell type and maximum cell density. Samples were measured fluorometrically by monitoring the increase in fluorescence at a wavelength of 590 nm using an excitation wavelength of 560 nm. Cell viability was consequently calculated using the following equation:

$$\text{Cell viability} = (\Delta\text{Sample} - \Delta\text{Blank}) / (\Delta\text{Control} - \Delta\text{Blank}) \times 100 \quad (7)$$

ΔSample = absorbance of treated cells 560 − absorbance of treated cells 590;

ΔBlank = mean absorbance of blank 560 − mean absorbance of blank 590;

ΔControl = mean absorbance of untreated control 560 − mean absorbance of untreated control 590.

### 2.13. Statistical analysis

Data were analysed and graphically presented by using GraphPad Prism™ version 9 (GraphPad software Inc., San Diego, CA, USA). The percentage CV was calculated and used for interpretation of the method validation results. Data were tested for normality by using the Shapiro–Wilks test. Statistical significance between 2D cell cultures and the 3D

bioprinted hydrogel scaffolds were determined by two way-ANOVA with Tukey's post hoc analysis and set at $p \leqslant 0.05$.

## 3. Results

### 3.1. Printability of the hydrogel biomaterial ink

All four chosen hydrogel blends from the printability evaluation were capable of being extruded at an extrusion pressure lower than 100 kPa using nozzle diameters between 25 and 27G and strand widths varying depending on the viscosity of hydrogel (supplementary material, tables S1–S3). Table 1 lists the results of the hydrogel blend of alginate 7% + gelatine 8% (w/v) with the highest print accuracy. When the alginate concentration increased, the strand width decreased. Therefore, the POI also increased at higher alginate concentrations. At higher print pressures, the increase in extrusion speed had a greater impact on strand width thus on print accuracy. At the fastest print speeds, adequate prints were not possible for reasons of nozzle gauge and pressure extruding too much hydrogel. From the entire study, the lowest ranked POI was $0.76 \pm 0.17$ (25G, 70 kPa, 6 mm $s^{-1}$) which resulted from a printed line width of $1.38 \pm 0.32$ mm, whereas the highest possible POI of $0.92 \pm 0.09$ was found with the 27G nozzle at 40 kPa and 8 mm $s^{-1}$ print speed, resulting in a line width of $0.39 \pm 0.04$, this is shown in bold in table 1. For the 7% alginate + 8% gelatine (w/v) hydrogel ratio tested, the POI suggested that the optimum parameters were: 27G nozzle, 40 kPa printing pressure and 8 mm $s^{-1}$ printing speed.

### 3.2. Mechanical traits of the hydrogel biomaterial ink

From the results obtained during the porosity study, it became clear that most of the hydrogel formulations indicated acceptable porosity, with the alginate 7% + gelatine 8% (w/v) hydrogel having the highest degree of porosity with $34.57 \pm 9\%$. No statically significant differences were evident (figure 1(A)). The printed scaffolds were incubated in two different media to determine their degradation in both different mediums and can be seen in figure 1(B) as degradation percentage vs time. DMEM media was an important medium to assess because when incorporated with the A375 cells the hydrogel scaffold will be supplemented with DMEM media to supply nutrients to cells. Alginate hydrogels follow a degradation process that involves the loss of divalent ions into surrounding media [50]. Whereas gelatine holds a thermally reversible ability that permits it to solidify at lower temperatures and gradually degrade into the surrounding medium at higher temperatures [21]. The alginate 7% + gelatine 8% (A7G8 in figures 1(A) and (B)) indicated a more gradual degradation rate in both $dH_2O$ and DMEM with percentages of $6.53 \pm 2.40\%$ and $4.33 \pm 2.52\%$ after 24 h, $11.06 \pm 2.42\%$ and $7.72 \pm 3.12\%$ after 48 h and finally $16.72 \pm 3.015\%$ and $26.64 \pm 15.41\%$ after 168 h.

The swelling efficiency of 10 of the optimised alginate and gelatine hydrogel printed scaffolds with crosslinking was evaluated in $dH_2O$ solution, and the results are given in figure 1(D) illustrated as weight gained vs time. The alginate gelatine scaffolds displayed a high expansion ratio, indicating the minimum solid property, leading to more water uptake. The weight of scaffold at 0 min was 0.26 g with an increase in weight of the scaffold after 15 min $0.69 \pm 0.09$ g, and after 30 min $0.79 \pm 0.23$ g results are depicted as mean and SD, rendering a percentage swelling ratio of 68.84% after 15 min and 78.51% after 30 min. Sodium citrate 4% (w/v) resulted in complete de-gelation of the scaffold after 30 min (figure 1(E)).

### 3.3. Cell-laden 3D hydrogel scaffold printing

A 10 mm × 10 mm × 0.8 mm grid was designed in Fusion 360 CAD software and was used as the design for the cell-laden scaffold. We found that 1:5 ratio of media to hydrogel showed uniform cell distribution and did not affect the hydrogel viscosity or extrudability. Samples were then printed using 27G nozzles with the BioX bioprinter using its in-built cleanroom environment. The print head was heated to 37 °C and the print bed to 10 °C and the scaffolds were printed. Once the scaffolds were printed, the samples were crosslinked with 4% (w/v) $CaCl_2$. DMEM media were added to each well and cells included in the 3D printed structures were cultured for 48 h. Cells quantified by the resazurin assay was done in triplicate and averaged results are shown as the relative fluorescence units for each plate with background debris already excluded (figure 2(A)). The results indicated that cells in the control group which was grown on 2D cell culture in media compared to the cells in 3D bioprinted hydrogel scaffolds indicated a higher intensity of fluorescence absorbance than that of the 2D cultured cells. The A375 cells were well distributed within the printed scaffold (figure 2(B)) and maintained their characteristic morphology. After 48 h cell numbers increased, cell distribution was maintained and there were no significant changes in cellular morphology visually observed (figure 2(C)).

### 3.4. Method validation

In the method validation part of this study, we followed a quasi-quantitative approach and focussing on specificity, precision, and sensitivity. In this study, specificity was defined in terms of how well the population of cells of interest could be separated and distinguished from the hydrogel particles [56]. The first important step was to characterise the scatter profile, including the complexity and size of the alginate–gelatine hydrogel particles. In addition, it was important to determine the gating strategy to be used when analysing gel and de-gelated gel samples. Figure 3(A)

**Table 1.** Printability of the hydrogel biomaterial ink. The effect of printing parameters on strand thickness and POI of alginate 7% + gelatine 8% (w/v) formulation. Strand width and POIs are indicated as mean ± standard deviations. The bold text indicated the optimum print parameters.

| | Hydrogel concentration alginate 7% + gelatine 8% | | |
|---|---|---|---|
| Printing parameters | Average Strand width (mm) | Average POI | Printing accuracy (%) |
| 25G nozzle, 100 kPa, 8 mm $s^{-1}$ | 1.35 ± 0.31 | 0.78 ± 0.17 | 23.25 |
| 25G nozzle, 70 kPa, 6 mm $s^{-1}$ | 1.38 ± 0.32 | 0.76 ± 0.17 | 22.81 |
| 25G nozzle, 50 kPa, 4 mm $s^{-1}$ | 0.81 ± 0.12 | 0.80 ± 0.12 | 37.88 |
| 25G nozzle, 40 kPa, 4 mm $s^{-1}$ | 0.75 ± 0.12 | 0.81 ± 0.12 | 40.84 |
| 27G nozzle, 100 kPa, 12 mm $s^{-1}$ | 1.26 ± 0.14 | 0.85 ± 0.10 | 23.98 |
| 27G nozzle, 70 kPa, 10 mm $s^{-1}$ | 1.13 ± 0.09 | 0.85 ± 0.07 | 24.80 |
| 27G nozzle, 50 kPa, 8 mm $s^{-1}$ | 0.51 ± 0.09 | 0.82 ± 0.14 | 60.90 |
| **27G nozzle, 40 kPa, 8 mm $s^{-1}$** | **0.39 ± 0.04** | **0.92 ± 0.09** | **77.34** |

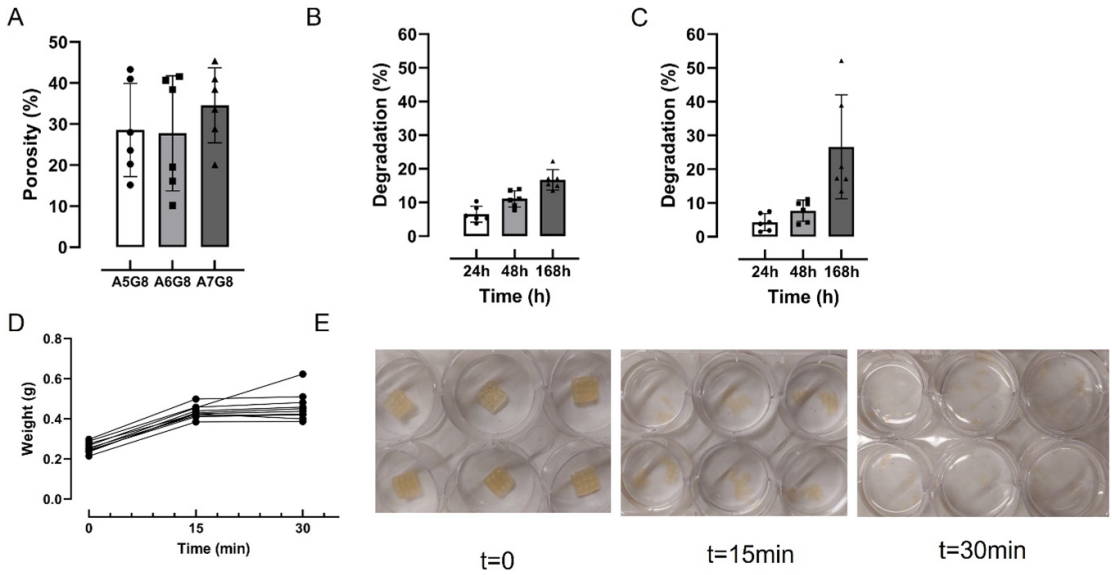


**Figure 1.** Mechanical traits of the hydrogel biomaterial ink. (A) Porosity (%) of the different weight ratios of alginate and gelatine hydrogel blends. Six different alginate and gelatine blends were investigated as possible bioinks with alginate and gelatine in different weight ratios: alginate 5% + gelatine 8% (w/v) alginate 6% + gelatine 8% (w/v) alginate 7% + gelatine 8% (w/v). Results are presented as mean ± standard deviation (SD) with the bars, whereas individual data points are presented by the symbols ($n = 6$). (B) Degradation profiles of the alginate 7% (w/v) + gelatine 8% (w/v) hydrogels in two different media including $dH_2O$ and (C) DMEM cell culture media over a time period of 24 h, 48 h and 168 h. Results are presented as mean ± standard deviation (SD) with the bars, whereas individual data points are presented by the symbols ($n = 6$). *indicates statistical significance ($p \leqslant 0.05$). (D) Swelling behaviour of alginate 7% (w/v) + gelatine 8% (w/v) 3D printed scaffolds in $dH_20$ indicating weight gain at 0-, 15- and 30-min. Results are presented as individual data points ($n = 10$). (E) Representative photographs of alginate–gelatine hydrogel scaffolds being de-gelated with trisodium citrate ($Na_3C_6H_5O_7$) 4% (w/v) directly after cross-linking, after 15 min of incubation and after 30 min of incubation.

illustrates representative density plots of the diluted hydrogel and is compared to the diluted de-gelated hydrogel (figure 3(B)). A marked difference in the scatter profile can be seen between the hydrogel and the de-gelated hydrogel. De-gelation resulted in a small population with size (FSC) below 60 000 and complexity (SSC) below 0 (well below the analytical threshold of the FACSLyric) that could be gated from the analysis. A gating strategy could be implemented to exclude the de-gelated gel particles.

In the next step, 3D bioprinted hydrogels with cells were used to determine whether the hydrogel will obscure the cell analysis. The 3D bioprinted scaffolds containing cells were grown for up to 48 h and then de-gelated (figure 3(D)) and compared with 2D culture cells grown for 48 h and suspended in PBS (figure 3(C)). A total number of 10 000 events were counted for both groups—representative FSC/SSC plots and bivariate FITC and PI plots. The gating strategy used for cell analysis of induced apoptosis in this study was a two-parameter gating strategy. This data could be visualized where the density plot is split into four quadrants, quantifying the cells single positive for each marker and both double negative and double positive. Apoptotic cells positive for Annexin V can be seen in the bottom right quadrant and dead cells positive for both Annexin V and PI in the top right quadrant. Live cells are negative for both stains. No clear differences could be seen in the FSC/SSC profile of the 2D cultured cells in PBS (figure 3(C)) and the de-gelated 3D bioprinted hydrogel scaffold with A375 cells (figure 3(D)). There

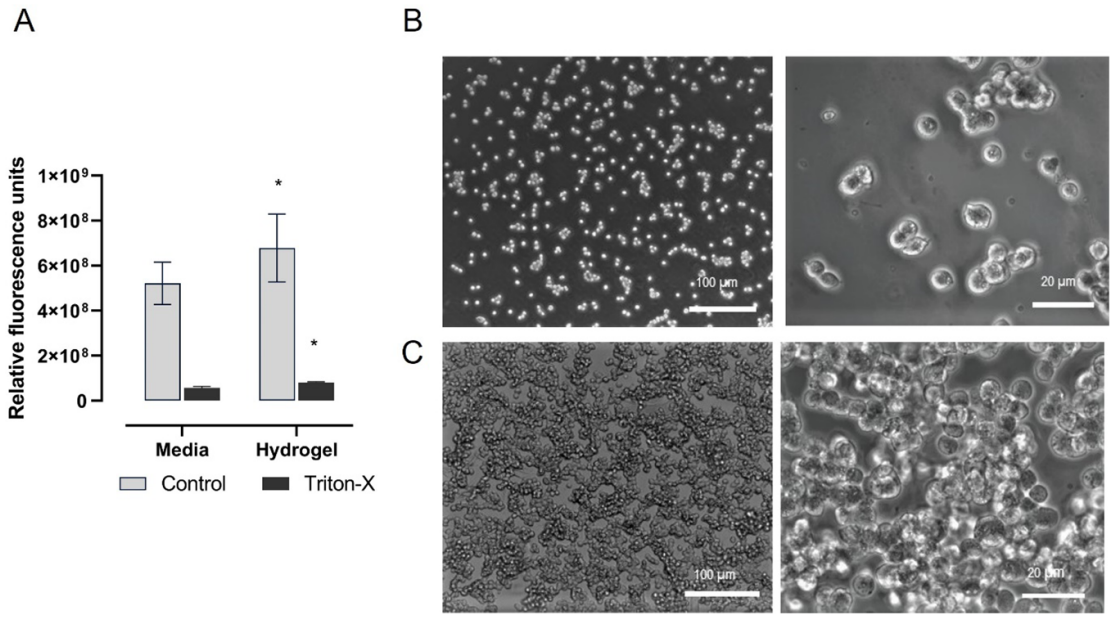


**Figure 2.** Bioprinting of A375 cell-laden alginate 7% + gelatine 8% (w/v) hydrogel scaffolds. (A) Resazurin cell viability assay measured absorbance of resazurin of A375 cells in media and cells 3D printed in alginate–gelatine hydrogel. *indicates statistically significant differences from media ($p \leqslant 0.05$) $n = 6$. (B) Observing distribution of cells after printing $1 \times 10^6$ cells into a two-layered scaffold. About 10 times magnification directly after printing, and 40 times magnification directly after printing. (C) is the same scaffold and distribution of cells after 48 h of incubation in DMEM cell culture medium, and 40 times magnification of cells after 48 h.

was no interference of the hydrogel with the Annexin V and PI staining, as background fluorescence of both samples were low with values below 2%. The percentages in all the quadrants did not differ statistically significantly when unstained cells in PBS were compared with unstained cells in the de-gelated hydrogel. Cells could be accurately detected and distinguished from the de-gelated hydrogel with no data deconvolution needed. This result differed from that of Gretzinger's [34], research where data deconvolution was integral to their analysis. The results also differed from the beads analysed, where accurate percentages of beads could not be distinguished due to interference of gel material. Even though accurate percentage of beads could not be captured, the gel had no influence on the SSC geometric mean parameters (supplementary material). The beads were however extremely small (2–3 µm), whereas A375 melanoma cells have an average size of 50–70 µm. Whereas beads could not be accurately removed from the gel material during preparation, cells could be successfully isolated as is evident from the FSC/SSC plots (figures S3 and 3). The specificity of the method was confirmed as the population of interest could be identified and quantified. Additionally, it was proven that the de-gelating solution had no effect on cell viability, similar to results previously reported [59].

Precision, also known as reproducibility or repeatability, is the degree to which repeated measurements can give the same results under unchanged conditions. Thus, precision quantifies the variability of an analytical result as a function of operator, method manipulations, and day-to-day environment. Statistical analysis of data generated is essential to demonstrate assay precision and to presented it as percentage CV. The precision approval criteria for cell-based assays are usually between 10% and 25% for the CV [56, 60]. The intra-assay precision (reproducibility) describes the variation of results within a data set obtained from the same experiment. Inter-assay precision (repeatability) is intermediate precision expressed within-laboratory variations, including different days, different equipment, or different operators [61]. The inter-assay precision was determined through analysing the same sample twice on different days and different batches of hydrogel. Results from both the calibration beads (supplementary material) and cells proved precision. Table 2 lists the CV% calculated for the inter and intra assay precision. The method conformed to the precision criteria of CV% below 10%–25%, or 35% for low fluorescence events [56].

Sensitivity is the precision and accuracy of the measurement of rare events or dim agents. Stated differently, it is the ability of the assay to distinguish fluorescence signal from the background and precisely measure low amounts of the population of interest. Firstly, fluorescent minus one staining was done to determine the amount of background (figure 4). This was important to confirm

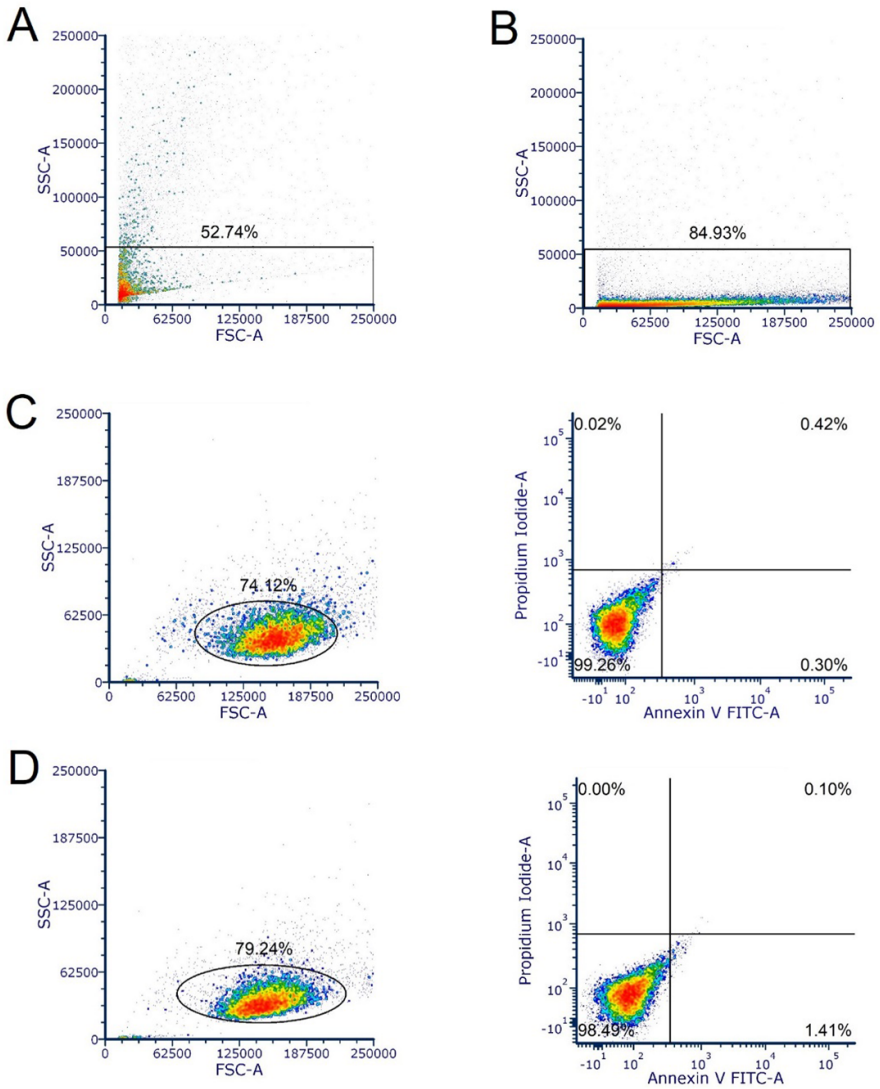


**Figure 3.** Method validation—specificity. Analysis of diluted alginate 7% + gelatine 8% (w/v) hydrogel in phosphate-buffered saline (PBS) to determine the interference with flow cytometric analysis. Illustrated representative density plots of forward scatter (FCS) indicating size and side scatter (SSC) indicating complexity of (A) gel diluted in PBS and (B) de-gelated gel in PBS. Interference of hydrogel when A375 cells are analysed with flow cytometry. FSC/SSC and fluorescence bivariate density plots of (C) unstained and untreated cells in PBS vs (D) unstained and untreated cells in de-gelated hydrogel.

**Table 2.** Precision of the Annexin V/PI flow analysis method of A375 3D bioprinted in hydrogel scaffold. Summary of the coefficient of variation (CV%) of intra and inter assay precision of cells 3D bioprinted in hydrogel.

| | Intra assay precision CV% | Inter assay precision CV% |
|---|---|---|
| Live | 0.97 | 0.70 |
| Dead | 26.47 | 27.99 |
| Early apoptosis | 17.20 | 34.39 |
| Late apoptosis | 1.61 | 16.83 |

if non-specific staining of gel material (particles) occur when Annexin-V or PI is added to the samples. The minimum events that counted as true events and not background were above 200 events (2% when 10 000 events were used). Only the lower left (early apoptosis), upper right (late apoptosis) and upper left (dead cells) quadrants were considered as explained by the gating strategy. For the unstained cells in no background could be seen in the FITC or PE channels (figure 4(A)). When FITC alone is added to the cells, the background of both channels increases, and a low percentage of dead cells can be observed (figure 4(B)). This is expected as some cell death occurs in normal processing of the sample. When PI alone is added to the cells (figure 4(C)), only the PI fluorescence increases, with a small number of dead cells visible. When both dyes are added to the cells (figure 4(D)), the fluorescence increases in the FITC channel with some detectable and quantifiable amounts of apoptotic and dead cells. The summary statistics is listed in the supplementary material (table S17). In terms of the sensitivity of the assay, in the sample used as the negative control (untreated but stained cells), some

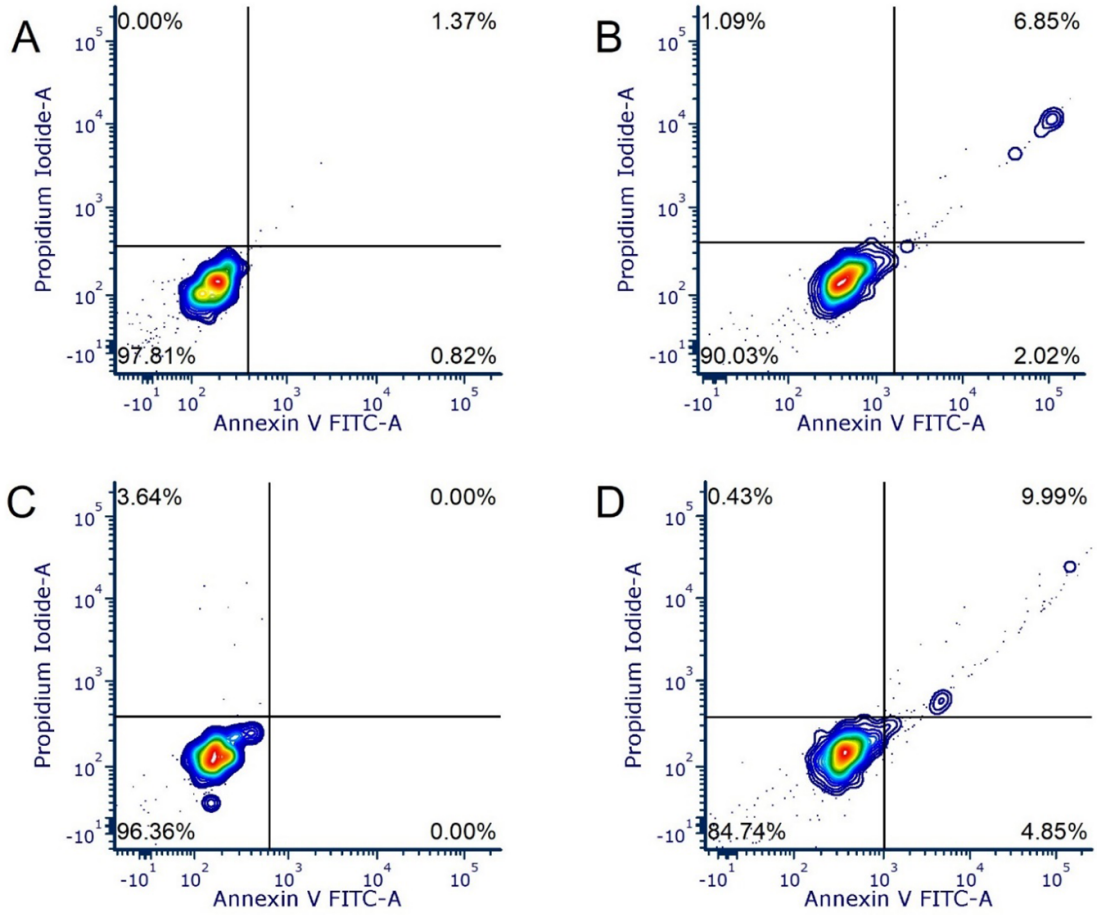


**Figure 4.** Method validation—sensitivity determined by fluorescence minus one staining to determine the amount of background staining in the presence of hydrogel. Representative flow cytometry contour plots of untreated cells that was (A) unstained (B) stained with Annexin V-FITC only (C) stained with propidium iodide (PI) only (D) and stained with both Annexin V-FITC and PI. ($6 \times 10^4$ cells per scaffold cultured for 48 h).

dead, early apoptotic and late apoptotic events can be detected. This is not unusual and is observed for most cell viability assays. It is usually factored into the cell viability equation [62]. The gel therefore did not interfere and cause non-specific fluorescence that could interfere with the sensitivity of the assay.

In the next step the untreated and stained cells as well as etoposide treated were compared in terms of a low cell count vs a high cell count. There were no clear differences in terms of the visual observation when low cell counts (figure 5(A) or (C)) were compared to high cell counts figure 5(B) or (D). Similar results were found for the calibration beads (supplementary material). The number of events considered as background in the lower left, upper left and upper right, were below 200 (or 2%). The summary statistics indicated that all the events in the relevant quadrants were below 2% (supplementary material, table S18). There were no statistically significant differences between the low cell count and the high cell count. Lastly the LOD of an analytical method is an important parameter when quantitative measurements have been taken. The LOB and LLOQ calculated are reflected in table 3.

### 3.5. Anti-cancer activity of etoposide on 3D bioprinted A375 melanoma cells

In the last part of the study, we compared two approaches in order to assess the efficacy of etoposide in melanoma cells cultured in a 3D bioprinted scaffold and to compare the validated method's results of induced apoptosis with a traditional method of analysing cell viability, namely resazurin plate-reader assay. In order to study whether the anti-cancer drug etoposide caused cell death and apoptosis, an Annexin V/PI staining technique followed by flow cytometry analysis was used. Annexin V is a protein that can adhere to phosphatidylserine (PS) translocated to the cell membrane's outer surface, and can be used to observe apoptotic cells by marking it with a fluorescent chemical (e.g. FITC). Because this protein binding may be recognized on the surface of necrotic cells, a second non-vital dye PI is added to enable the simultaneous detection of two distinct cells [63]. Annexin V and PI have been used widely for various apoptosis detection and drug efficacy studies [64–66]. A375 melanoma cells cultured in 2D and cultured in the 3D in the alginate–gelatine hydrogel scaffolds were treated with different concentrations

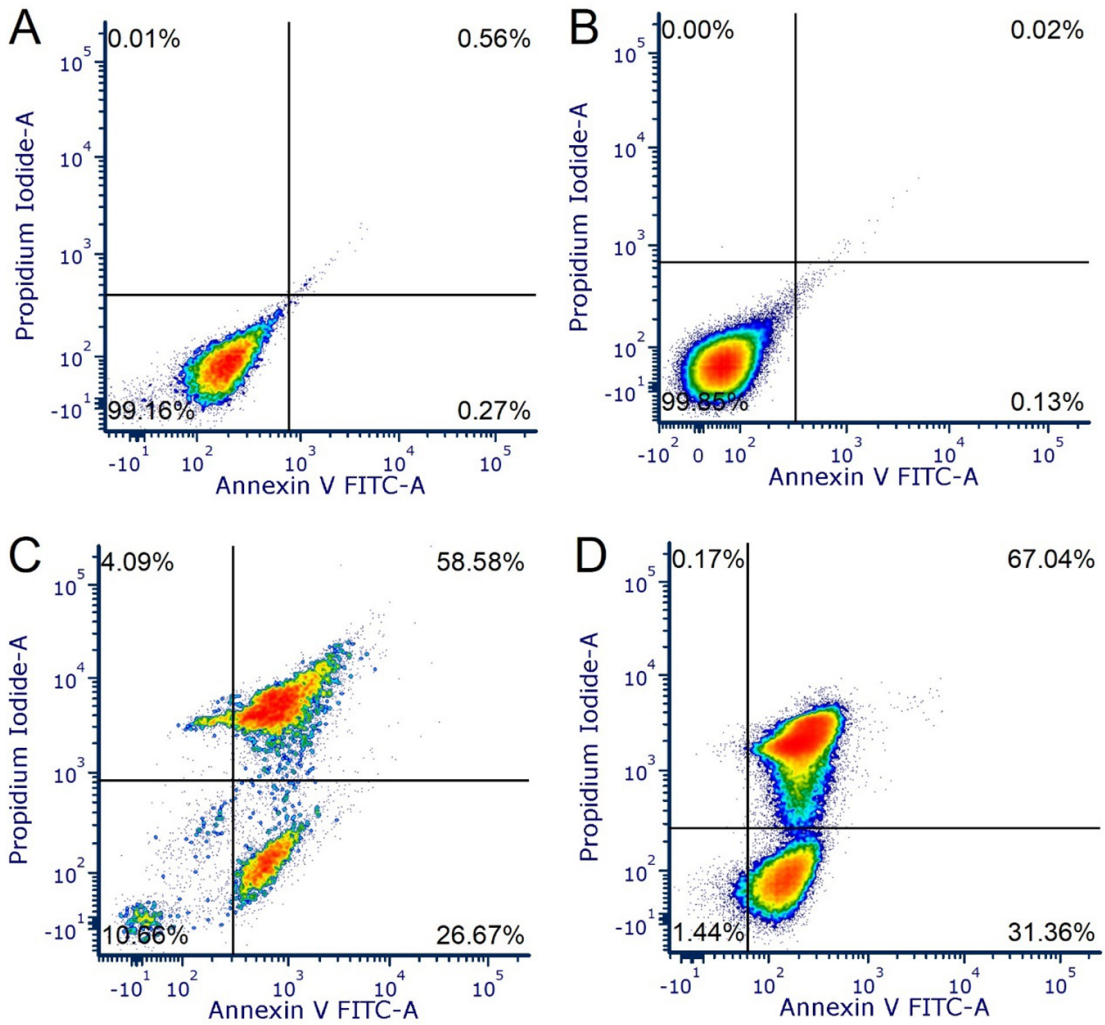


**Figure 5.** Method validation—sensitivity measured as the accuracy of determining the population of interest. Representative density plots of 3D bioprinted A375 cells in the presence of hydrogel that was (A) untreated and low cell count with 10 000 events and (B) high cell count with 100 000 events and cells (C) treated with 100 μM etoposide and low cell count with 10 000 events and (D) high cell count with 100 000 events. ($6 \times 10^4$ cells per scaffold cultured for 48 h).

of etoposide for 4 h and then stained and analysed. Figure 6 illustrates the representative density plots including the quadrant gates of cells analysed; viable cells that excluded both Annexin V and PI (Annexin V−/PI−), bottom left, early apoptotic cells that were only stained with Annexin V (Annexin V+/PI−), bottom right, late apoptotic cells that were stained with both Annexin V and PI (Annexin V+/P+), top right, and necrotic cells that were only stained with PI (Annexin V−/PI+), top left. There were no obvious differences between the bivariate density plots, with a high percentage of treated cells presenting the late apoptosis.

When comparing the results from the 2D cell culture and 3D bioprinted hydrogel scaffold of A375 cells no statistically significant differences were calculated in terms of efficacy of the anti-cancer drug, etoposide (figure 6). Typically, drugs that have a minor effect on the viability of cells grown in 2D cell cultures will have little to no effect on 3D cell culture models, although the opposite may also be true; consequently, these methods are extremely useful for the development of assays to identify potential therapies. 3D cell culture models that more effectively replicate the *in vitro* microarchitecture of tumours can promote the clinical implementation of these preclinical outcomes [67].

**Table 3.** Method validation—measurement of sensitivity of the Annexin V/PI flow cytometry analysis of 3D bioprinted A375 cells in the presence of hydrogel in terms of the limit of detection. Results are presented as the calculated percentage limit of blank (LOB) and percentage lower limit of quantification (LLOQ).

| | LOB% of unstained cells | LLOQ% of stained, untreated cells |
|---|---|---|
| Dead | 1.06 | 2.12 |
| Early apoptosis | 1.44 | 2.46 |
| Late apoptosis | 3.90 | 4.90 |

In addition, it could be observed that there was no interference of the hydrogel with drug uptake and the

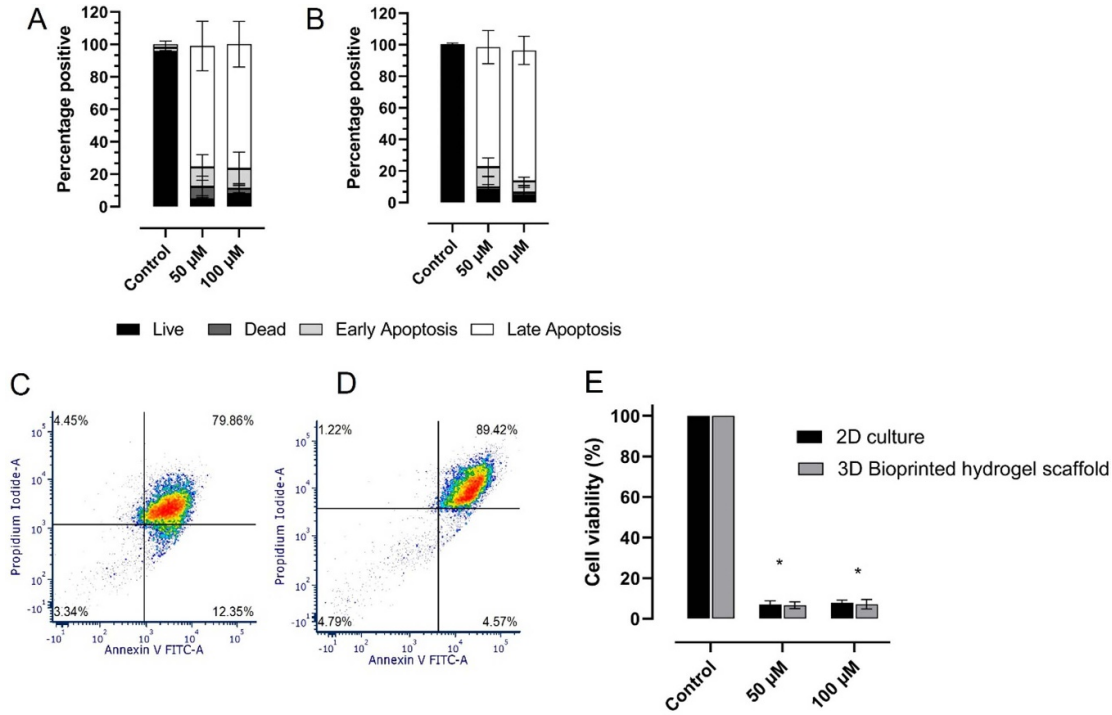


**Figure 6.** Method validation—anti-cancer activity and comparison of the flow cytometry method with the resazurin assay. Side-by-side comparison of histograms presenting the percentage positive cells in each quadrant of control (stained but untreated cells) and cells exposed to etoposide in concentrations of 50 µM and 100 µM for 4 h (A) cells cultured in 2D vs (B) cells cultured in 3D hydrogel scaffolds ($6 \times 10^4$ cells per scaffold cultured for 48 h). A total of 10 000 events were captured. Results are presented as mean ± SD ($n = 3$). Representative density plots of the effect of etoposide on (C) cells cultured in 2D treated with 100 µM (D) cells cultured in 3D hydrogel scaffolds treated with 100 µM. Viable cells—Annexin V-negative/PI-negative cells; early apoptotic cells—Annexin V-positive/PI-negative cells; late apoptotic cells—Annexin V-positive/PI-positive cells, necrotic cells—Annexin V-negative/PI-positive cells. (E) Bar graph presenting the percentage cell viability of A375 cells treated with etoposide in concentrations of 50 µM and 100 µM for 4 h analysed with the resazurin assay. Control is untreated cells. The histograms are representative for three independent experiments analysed in triplicate with accumulated average results. A375 melanoma cells cultured in 2D and cells bioprinted in 3D hydrogel. *indicates statistically significant differences compared to the control ($p \leqslant 0.05$).

analysis method. The percentage of live cells in both the 2D cell culture and the 3D bioprinted hydrogel scaffold control was above 95% with 94.84 ± 3.40% and 97.52 ± 0.87% respectively. The percentage dead cells were slightly higher for the 2D cell culture treated with etoposide than the 3D bioprinted hydrogel scaffold. The percentage dead cells were 7.82 ± 6.72% and 3.34 ± 2.31% for the 50 and 100 µM etoposide treated 2D cells, as opposed to 1.56 ± 1.74% and 1.65 ± 3.16% of the 3D bioprinted hydrogel scaffold of A375 cells. This difference was not statistically significant. In both the 2D cells and the A375 cells 3D bioprinted in hydrogel scaffolds the percentage of cells in early apoptosis were between 7% and 12% (50 µM etoposide 11.95 ± 7.89% and 12.72 ± 5.90% compared to 100 µM etoposide 12.25 ± 10.26% and 7.11 ± 2.65% for the 2D cells and 3D bioprinted cells respectively). Late apoptosis increased with 74.87 ± 15.20% and 76.11 ± 10.50% cells treated with 50 µM and 76.81 ± 14.01% and 82.98 ± 8.90% in cells treated with 100 µM etoposide in the 2D cells and 3D bioprinted cells respectively. These results differed statistically significantly from the control. The Annexin V/PI method could be used to accurately quantify the percentage of live, dead, early apoptotic and late apoptotic A375 cells bioprinted in a hydrogel scaffold.

### 3.6. Comparison of the flow cytometry method with the resazurin-based assay

Both etoposide treatment groups differed significantly from control but there was no additional advantage of quantifying four different endpoints in cell viability, compared to significant differences between the 2D and 3D cultured cells. The results observed from the micro-plate reader resazurin-based assay reflected similar results, compared to the flow cytometric analysis with the percentage of dead cells 7.02 ± 1.97% and 6.68 ± 1.66% in the 50 µM etoposide and 7.89 ± 1.30% and 7.15 ± 2.34% in the 100 µM etoposide treated 2D cells and 3D bioprinted A375 cells respectively (figure 6(F)). The Annexin V/PI flow cytometry method showed one endpoint of the resazurin assay. In addition, flow cytometry was able to report single-cell events, compared to the average result from all the cells combined given by the plate-reader assay.

## 4. Discussion

Three-dimensional bioprinting is a versatile technique for creating biomimetic tissue structures. The mechanical properties of biomaterials are an important parameter in regulating the behaviour of cell adhesion. In extrusion bioprinting, the mechanical properties of the hydrogel play an important role in determining the printed structure accuracy and cell viability [68, 69]. We evaluated different weight ratios of alginate–gelatine hydrogel blends cross-linked with $CaCl_2$ after bioprinting to form the basis of our bioink. Various studies have used alginate in combination with other polymers such as gelatine in tissue engineering and pneumatic extrusion [70, 71]. Suitable bioinks for the application of 3D cell printing should meet both the biological requirements and the requirements needed for good printability.

Various blends of alginate and gelatine were firstly evaluated in terms of their printability and printing parameters with the pneumatic extrusion-based BioX bioprinter from Cellink and then the hydrogels were characterised in terms of their mechanical traits with porosity, degradation and swelling property evaluations. Previous studies conducted by other researchers established the printability and biocompatibility of alginate and gelatine hydrogels with an alginate weight ratio ranging from 3%–7% (w/v) and gelatine weight ratio of 4%–8% (w/v) [50, 72–74]. In this study only four out of the six alginate and gelatine blends (alginate 7% + gelatine 8% (w/v), alginate 6% + gelatine 8% (w/v), alginate 5% + gelatine 8% (w/v), alginate 7% + gelatine 5% (w/v),) were suitable for 3D printing with the method investigated, in terms of nozzle diameter, pressure, printing speed and nozzle-printed distance. Taking into account the thinner strand widths and higher POI values, the optimised printing parameters were 27G nozzle, 40 kPa, 8 mm $s^{-1}$ print-head temperature of 37 °C and print-bed temperature of 10 °C rendering an average printing accuracy of 77.34%. Strand width results were strongly affected by polymer concentration, which confirmed the findings of previous studies [51, 52]. Di Giuseppe *et al* [49] reported that increasing the concentration of alginate led to more accurate printing, and higher concentration of gelatine reduced the printing accuracy, which is consistent with our findings where alginate 2% + gelatine 8% (w/v), alginate 2% + gelatine 5% (w/v) were not extrudable with a higher gelatine to alginate weight ratio. On the basis of the optimised printing parameters the chosen hydrogel blend was alginate 7% + gelatine 8% (w/v). Another study using a blend of 7% alginate and 8% gelatine found that the concentration of the hydrogel blend resulted in high printability, mechanical strength, and high cellular viability [49].

Next, we evaluated the mechanical traits of the hydrogel blends. The porosity of a hydrogel scaffold is important because it can influence nutrient supply, gas diffusion, metabolic waste removal, cell attachment and intracellular signalling [75]. The extent of porosity will also have a significant effect on the mechanical properties of the hydrogel scaffold, considering that stiffness of the scaffold is inversely proportional to porosity [76]. Though scaffolds possessing a porosity of that magnitude usually exhibit an extreme decrease in mechanical strength, a compromise between porosity and mechanical properties will have to be considered [77]. In this current study the chosen hydrogel blend of alginate 7% + gelatine 8% (w/v), had the highest degree of porosity with 34.57 ± 9%, indicating that there is a suitable amount of porosity, but it would not affect the scaffold stability.

Degradation and swelling studies are relevant for 3D bioprinting of constructs as these physical properties affect cell viability, proliferation, and the formation of new tissue. The observed swelling ratio was a balance between the uptake of water and the degradation rate of the alginate 7% + gelatine 8% hydrogel blend. Swelling ratio of the construct was 78.51% after 30 min and the same hydrogel reflected a more gradual degradation rate in both $dH_2O$ and DMEM. The degradation rate should match with the time necessary for desired tissue regeneration. Hence modulating the degradation rate is desired in this study. The degradation time of the alginate hydrogels can be controlled by adding sodium citrate to de-gelate the scaffold prior to analysis without harming cells. We added 4% (w/v) trisodium citrate to scaffolds to de-gelate and analyse the cell viabilities; after 30 min the scaffold was completely degraded. The same results have been reported by other studies and added to this, they reported that the sodium citrate used to accelerate degradation was helpful for the growth and proliferation of the printed cells, indicating that no harm is caused to cells [55, 59].

As observed, based on the cell viability studies rendering high cell viabilities of 87%–94%, the study confirmed that the alginate 7% + gelatine 8% hydrogel blend supported cellular viability. In another study utilising alginate and gelatine hydrogels to culture Schwann cells reported high cell viabilities on days 1, 4 and 7 of 87 ± 0.55%, 92.83 ± 0.46%, and 93.20 ± 0.52% respectively, indicating that the cells were slightly affected by shear force during printing, but survived for seven days and also confirming the biocompatibility of alginate and gelatine hydrogels [78]. Additionally, this hydrogel blend holds the potential of encapsulating different cell lines and promoting cell proliferation; thus facilitating use of these hydrogels for tissue-engineering applications

such as drug efficacy and toxicity testing for cancer research.

In drug discovery and drug delivery research there is a constant need for viable and reliable alternatives for *in vitro* drug efficacy and toxicity testing. Cell-based assays are critical in the pre-clinical drug discovery and development process with the advancements of 3D cell cultures, analytical assays require to be adapted [79]. Method validation is a series of tests intended to guarantee that an analytical method is suitable for its intended purpose and capable of producing useful and authentic analytical results [80]. Due to the use of an alginate-based bioink, cross-linking of the alginate scaffolds was accomplished after printing by ionic gelation. Hence de-gelation of the cell-laden scaffold was required prior to analysis. In the method validation, we followed a quasi-quantitative approach and focussing on specificity, precision and sensitivity. Method validation can be described as a series of tests meant to ensure that an analytical experimental setup is appropriate for its intended purpose and capable of producing useful and authentic analytical data. Specificity is the ability of a method/assay to identify or quantify a given determinant in the presence of other determinants or interfering compounds [56]. In this study specificity was defined in terms of how well the population of cells of interest could be separated and distinguished from the hydrogel particles. Gretzinger *et al* [34] developed a high throughput flow cytometric analysis method for determining cell proliferation in 3D printed scaffolds with CellTrace violet stain. They utilised a commercial alginate-based hydrogel with added nano-cellulose to improve shape fidelity. Yet in the flow cytometric analysis this caused interference with the signal of the flow cytometer, and data deconvolution had to be actualised. In this study the 3D bioprinted hydrogel scaffold consisted of 7% alginate and 8% gelatine and nano-cellulose was not needed for shape fidelity; therefore, interference of the fibres was eliminated. Although it was suspected that this hydrogel will obscure the signal of the flow cytometer less, it was still important to determine if whether deconvolution was needed and to what degree. Cells could be accurately detected and distinguished from the de-gelated hydrogel with no data deconvolution needed. This result differed from that of Gretzinger *et al*'s [34] research where data deconvolution was integral to their analysis. Specificity of the method was confirmed as the population of interest could be identified and quantified. Additionally, it was proven that the de-gelating solution had no effect on the cell viability, similar to results previously reported [59].

Evaluation of assay precision is an essential aspect of flow cytometry method validation. The precision within an assay is assessed by the similarity of findings when the same sample is repeatedly examined under the same circumstances. The acceptable accuracy range for cell-based assays is 10%–25%. For uncommon populations, greater inaccuracies of 30%–35% are often acceptable. Inter-precision quantifies the disparity between researchers, instruments, and facilities. When intra-assay precision has been obtained, inter-assay reproducibility variation must be assessed [61, 81]. The assay precision of unstained cells was in the accepted criteria range and determined sufficient reproducibility of the assay.

The assay's sensitivity is dependent upon the type of data/output produced; however, the objective is to minimise false positive and false negative findings. Typically, for quasi-quantitative evaluations in flow cytometry, this refers to the assay's capacity to identify and measure low numbers or dim fluorescence populations. For the Annexin-V/PI experiment for cells bioprinted in the A7G8 gel, it was essential to demonstrate that the gel material (particles) did not affect the number of events recorded (percentage of cells counted) or the fluorescence parameters' intensity (geometric mean MFI). CV values in the range of 20%–35% were deemed appropriate for biomarker techniques and were used in this investigation. The minimum number of occurrences classified as actual events and not considered background for this investigation was established at 200 events. Analytical sensitivity for these tests includes the LOD, the capacity to differentiate from the background LOB, and the LLOQ [56]. The LOB is the maximum visible analyte concentration predicted to be obtained when testing duplicates of a sample that contains no analyte, 95% of negative results are typically below this threshold [61]. The LOD is usually associated directly with the LOB. The LOD is the concentration at which 95% of recorded low concentrations of the sample are detected above the concentration of the blank, where 5% false positive and false negative rates are expected. The LLOQ is the lowest level of the measured analyte that can be identified (LOD) and whose total error meets a certain standard of accuracy. LLOQ will sometimes equal the LOD value but never fall below the LOD value. For the sensitivity parameters in this study, the LOB and LLOQ were calculated. The LOD and LLOQ values indicated that the flow cytometric analysis method can detect small changes in a sample with acceptable LOD and LLOQ values. Validation of this flow cytometric approach was accomplished with appropriate specificity, accuracy, and sensitivity for all compounds, and it is thus possible to detect and identify drug-induced apoptosis in the 3D bioprinted hydrogel scaffolds. In order to study whether the anti-cancer drug etoposide caused cell death and apoptosis, an Annexin V/PI staining technique was chosen as it has been used widely for various apoptosis detection and drug efficacy studies [64–66]. Annexin V is a protein that can adhere to PS translocated to the cell membrane's outer surface, and can be used to observe apoptotic cells by marking it with a fluorescent chemical (e.g. FITC). Because

this protein binding may be recognised on the surface of necrotic cells, a second non-vital dye PI is added to enable simultaneous detection of two distinct cells [63]. There were no obvious differences between the bivariate density plots, with a high percentage of treated cells presenting the late apoptosis. The high percentage of cells with late apoptosis was a typical finding for etoposide in cancer cells and was similar to other studies [57, 82]. Additionally, the analysis showed that the 3D bioprinted cells were slightly more sensitive to drug-induced apoptosis than the 2D cultured cells, although this finding was not statistically significant and has to be confirmed with additional studies.

Next the anti-cancer efficacy of etoposide was evaluated on the A375 melanoma cells cultured in 2D and 3D bioprinted scaffolds analysed by the flow cytometric validated method and compared with a fluorometrically based micro-plate reader method. Both analysis methods indicated that the etoposide had a significant effect on the viability of the cells at both concentrations (50 μM and 100 μM) of etoposide. There were no significant differences between the cells cultured in 2D when compared to the 3D bioprinted cells, but the flow cytometric method had shown more in-depth quantification of the efficacy of the evaluated drug on the cells. Sample preparation was less intensive, and one sample could be used to evaluate four different elements of the cells' viability at once such as live, dead, early apoptosis and late apoptosis. Flow cytometry offers the additional advantage of single-cell analysis, whereas fluorescence-based plate reader assays have the assumption of general equilibrium over all the cells [83]. It was concluded that the Annexin V/PI flow cytometry method can be used to detect and identify drug-induced apoptosis in 3D bioprinted hydrogel scaffolds.

## 5. Conclusions

The aim of this study was to develop a flow cytometry-based analytical strategy for the quantification of apoptosis with Annexin V and PI staining in 3D-bioprinted hydrogel cell scaffolds to be used in drug efficacy evaluations. In the validation method evaluating specificity of the analysis (determining how well the cell populations of interest can be separated and distinguished from gel particles) data deconvolution was not needed as the hydrogel particles did not interfere with the cell analysis. Precision and sensitivity of the analytical method showed satisfactory results inside the accepted criteria range. The method could accurately detect drug induced apoptosis, similar to 2D cell cultures and results were comparable to a standard fluorescence resazurin assay. Therefore, the method was concluded to be suited for analysis of 3D cell laden hydrogel scaffolds. The model presented here provides an alternative to conventional 2D *in vitro* melanoma models, with the advantages of a validated flow cytometry analysis method of studying drug induced apoptosis with multiple parameters on single cell level.

## Data availability statement

All data that support the findings of this study are included within the article (and any supplementary files).

## Funding

This work is based on the research supported wholly by the National Research Foundation of South Africa (NRF Competitive Programme for Rated Researchers, Ref.: SRUG200421515268); and opinions, findings and conclusions or recommendations expressed in any publication generated by the NRF-supported research are those of the author(s) alone; the NRF accepts no liability whatsoever in this regard.

## Conflict of interest

The authors confirm that there are no known conflicts of interest associated with this publication.

## Author contributions

Maryke de Villiers: Methodology, Investigation, Formal analysis, Writing—original draft, Visualization, Validation. Lissinda du Plessis: Conceptualization, Funding, Supervision, Resources, Methodology, Investigation, Formal analysis, Writing—original draft, Visualization, Validation, Data curation.

## ORCID iD

Lissinda H Du Plessis https://orcid.org/0000-0003-0954-2976

## References

[1] Griffith L G and Swartz M A 2006 Capturing complex 3D tissue physiology *in vitro Nat. Rev. Mol. Cell Biol.* **7** 211–24
[2] Pampaloni F, Reynaud E G and Stelzer E H K 2007 The third dimension bridges the gap between cell culture and live tissue *Nat. Rev. Mol. Cell Biol.* **8** 839–45
[3] Breslin S and O'Driscoll L 2013 Three-dimensional cell culture: the missing link in drug discovery *Drug Discov. Today* **18** 240–9
[4] Samadian H *et al* 2021 3D bioprinting technology to mimic the tumor microenvironment: tumor-on-a-chip concept *Mater. Today Adv.* **12** 100160
[5] Augustine R, Kalva S N, Ahmad R, Zahid A A, Hasan S, Nayeem A, McClements L and Hasan A 2021 Bioprinted cancer models: revolutionizing personalized cancer therapy *Transl. Oncol.* **14** 101015
[6] Kang H-W, Lee S J, Ko I K, Kengla C, Yoo J J and Atala A 2016 A 3D bioprinting system to produce human-scale tissue constructs with structural integrity *Nat. Biotechnol.* **34** 312–9

[7] Ding T and Zang H 2023 Novel biological insights revealed from the investigation of multiscale genome architecture *Comput. Struct. Biotechnol. J.* **21** 312–25
[8] Riss T and Trask O J 2021 Factors to consider when interrogating 3D culture models with plate readers or automated microscopes *In Vitro Cell. Dev. Biol. Anim.* **57** 238–56
[9] Ashammakhi N, Hasan A, Kaarela O, Byambaa B A, Sheikhi A, K A, Gaharwar A K and Khademhosseini A 2019 Advancing frontiers in bone bioprinting *Adv. Healthcare Mater.* **8** 1801048
[10] Murphy S V and Atala A 2014 3D bioprinting of tissues and organs *Nat. Biotechnol.* **32** 773
[11] Datta P, Dey M, Ataie Z, Unutmaz D and Ozbolat I T 2020 3D bioprinting for reconstituting the cancer microenvironment *npj Precis. Oncol.* **4** 1–13
[12] Koçak E, Yıldız A and Acartürk F 2021 Three dimensional bioprinting technology: applications in pharmaceutical and biomedical area *Colloids Surf.* B **197** 111396
[13] Kim J H, Seol Y-J, Ko I K, Kang H-W, Lee Y K, Yoo J J, Atala A and Lee S 2018 3D bioprinted human skeletal muscle constructs for muscle function restoration *Sci. Rep.* **8** 1–15
[14] Landers R, Hübner U, Schmelzeisen R and Mülhaupt R 2002 Rapid prototyping of scaffolds derived from thermoreversible hydrogels and tailored for applications in tissue engineering *Biomaterials* **23** 4437–47
[15] Pagnotta G, Kalia S, Di Lisa L, Cicero A F, Borghi C and Focarete M L 2022 Progress towards 3D bioprinting of tissue models for advanced drug screening: *in vitro* evaluation of drug toxicity and drug metabolism *Bioprinting* **27** e00218
[16] Sharifi M, Bai Q, Babadaei M M N, Chowdhury F, Hassan M, Taghizadeh A, Derakhshankhah H, Khan S, Hasan A and Falahati M 2021 3D bioprinting of engineered breast cancer constructs for personalized and targeted cancer therapy *J. Control. Release* **333** 91–106
[17] Derakhshanfar S, Mbeleck R, Xu K, Zhang X, Zhong W and Xing M 2018 3D bioprinting for biomedical devices and tissue engineering: a review of recent trends and advances *Bioact. Mater.* **3** 144–56
[18] Shah P P, Shah H B, Maniar K K and Özel T 2020 Extrusion-based 3D bioprinting of alginate-based tissue constructs *Proc. CIRP* **95** 143–8
[19] Luo Z, Mu X and Zhang Y S 2022 Biomaterials for bioprinting *Bioprinting* (London: Academic, Elsevier) pp 51–86
[20] Raees S *et al* 2023 Classification, processing, and applications of bioink and 3D bioprinting: a detailed review *Int. J. Biol. Macromol.* **232** 123476
[21] Jiang T *et al* 2019 Engineering bioprintable alginate/gelatin composite hydrogels with tunable mechanical and cell adhesive properties to modulate tumor spheroid growth kinetics *Biofabrication* **12** 015024
[22] Łabowska M B, Cierluk K, Jankowska A M, Kulbacka J, Detyna J and Michalak I 2021 A review on the adaption of alginate-gelatin hydrogels for 3D cultures and bioprinting *Materials* **14** 858
[23] Chimene D, Lennox K K, Kaunas R R and Gaharwar A K 2016 Advanced bioinks for 3D printing: a materials science perspective *Ann. Biomed. Eng.* **44** 2090–102
[24] Guvendiren M, Molde J, Soares R M and Kohn J 2016 Designing biomaterials for 3D printing *ACS Biomater. Sci. Eng.* **2** 1679–93
[25] Liu T, Delavaux C and Zhang Y S 2019 3D bioprinting for oncology applications *J. 3D Print. Med.* **3** 55–58
[26] Mahendiran B, Muthusamy S, Sampath S, Jaisankar S N, Popat K C, Selvakumar R and Krishnakumar G S 2021 Recent trends in natural polysaccharide based bioinks for multiscale 3D printing in tissue regeneration: a review *Int. J. Biol. Macromol.* **183** 564–88
[27] Flores-Torres S *et al* 2021 Alginate–gelatin–matrigel hydrogels enable the development and multigenerational passaging of patient-derived 3D bioprinted cancer spheroid models *Biofabrication* **13** 025001
[28] Edmondson R, Broglie J J, Adcock A F and Yang L 2014 Three-dimensional cell culture systems and their applications in drug discovery and cell-based biosensors *Assay Drug Dev. Technol.* **12** 207–18
[29] Bhatia S N and Ingber D E 2014 Microfluidic organs-on-chips *Nat. Biotechnol.* **32** 760–72
[30] Koch M and Włodarczyk-Biegun M K 2020 Faithful scanning electron microscopic (SEM) visualization of 3D printed alginate-based scaffolds *Bioprinting* **20** e00098
[31] Belfiore L *et al* 2021 Generation and analysis of 3D cell culture models for drug discovery *Eur. J. Pharm. Sci.* **163** 105876
[32] Booij T H, Price L S and Danen E H 2019 3D cell-based assays for drug screens: challenges in imaging, image analysis, and high-content analysis *SLAS Discov.: Adv. Life Sci. R&D* **24** 615–27
[33] Joshi P and Lee M-Y 2015 High content imaging (HCI) on miniaturized three-dimensional (3D) cell cultures *Biosensors* **5** 768–90
[34] Gretzinger S, Beckert N, Gleadall A, Lee-Thedieck C and Hubbuch J 2018 3D bioprinting–flow cytometry as analytical strategy for 3D cell structures *Bioprinting* **11** e00023
[35] Lee D W, Yi S H, Jeong S H, Ku B, Kim J and Lee M Y 2013 Plastic pillar inserts for three-dimensional (3D) cell cultures in 96-well plates *Sens. Actuators* B **177** 78–85
[36] Florczyk S J, Kievit F M, Wang K, Erickson A E, Ellenbogen R G and Zhang M 2016 3D porous chitosan–alginate scaffolds promote proliferation and enrichment of cancer stem-like cells *J. Mater. Chem.* B **4** 6326–34
[37] Hodzic E 2016 Single-cell analysis: advances and future perspectives *Bosn. J. Basic Med. Sci.* **16** 313–4
[38] Carmen J, Burger S R, McCaman M and Rowley J A 2012 Developing assays to address identity, potency, purity and safety: cell characterization in cell therapy process development *Regen. Med.* **7** 85–100
[39] Wlodkowic D, Skommer J and Darzynkiewicz Z 2009 Flow cytometry-based apoptosis detection *Apoptosis Methods and Protocols* ed P Erhardt and A Tothedn (Hatfield: Springer) pp 19–32
[40] Alvarez-Barrientos A, O'Connor J E, Castillo R N, Moreno A M and Prieto P 2001 Use of flow cytometry and confocal microscopy techniques to investigate early $CdCl_2$-induced nephrotoxicity *in vitro Toxicol. In Vitro* **15** 407–12
[41] Vermes I, Haanen C and Reutelingsperger C 2000 Flow cytometry of apoptotic cell death *J. Immunol. Methods* **243** 167–90
[42] Koopman G, Reutelingsperger C P, Kuijten G A, Keehnen R M, Pals S T and Van Oers M H 1994 Annexin V for flow cytometric detection of phosphatidylserine expression on B cells undergoing apoptosis *Blood* **84** 1415–20
[43] Vermes I, Haanen C, Steffens-Nakken H and Reutellingsperger C 1995 A novel assay for apoptosis flow cytometric detection of phosphatidylserine expression on early apoptotic cells using fluorescein labelled Annexin V *J. Immunol. Methods* **184** 39–51
[44] Torregrosa G, Oriola D, Trivedi V and Garcia-Ojalvo J 2022 Single-cell Bayesian deconvolution (arXiv:2202.06325)
[45] Avila Cobos F, Alquicira-Hernandez J, Powell J E, Mestdagh P and De Preter K 2020 Benchmarking of cell type deconvolution pipelines for transcriptomics data *Nat. Commun.* **11** 5650
[46] Ford R J and Becker F F 1982 The characterization of trypan blue-induced tumors in Wistar rats *Am. J. Pathol.* **106** 326–31
[47] Chung J H, Naficy S, Yue Z, Kapsa R, Quigley A, Moulton S E and Wallace G G 2013 Bio-ink properties and printability for extrusion printing living cells *Biomater. Sci.* **1** 763–73
[48] Duan B, Hockaday L A, Kang K H and Butcher J T 2013 3D bioprinting of heterogeneous aortic valve conduits with alginate/gelatin hydrogels *J. Biomed. Mater. Res.* A **101** 1255–64

[49] Di Giuseppe M, Law N, Webb B, Macrae R A, Liew L J, Sercombe T B, Dilley R J and Doyle B J 2018 Mechanical behaviour of alginate-gelatin hydrogels for 3D bioprinting *J. Mech. Behav. Biomed. Mater.* **79** 150–7
[50] Li Z, Huang S, Liu Y, Yao B, Hu T, Shi H, Xie J and Fu X 2018 Tuning alginate-gelatin bioink properties by varying solvent and their impact on stem cell behaviour *Sci. Rep.* **8** 1–8
[51] Webb B and J D B 2017 Parameter optimization for 3D bioprinting of hydrogels *Bioprinting* **8** 8–12
[52] Hibbert M, Viljoen J M and Du Plessis L H 2023 Print parameter optimisation for a Pluronic F-127 and alginate hybrid hydrogel *Bioprinting* **30** e00257
[53] Cao D, Zhang Y, Cui Z, Du Y and Shi Z 2017 New strategy for design and fabrication of polymer hydrogel with tunable porosity as artificial corneal skirt *Mater. Sci. Eng.* C **70** 665–72
[54] Aldana A A, Valente F, Dilley R and Doyle B J 2021 Development of 3D bioprinted GelMA-alginate hydrogels with tunable mechanical properties *Bioprinting* **21** e00105
[55] Chawla D, Kaur T, Joshi A and Singh N 2020 3D bioprinted alginate-gelatin based scaffolds for soft tissue engineering *Int. J. Biol. Macromol.* **144** 560–7
[56] Selliah N, Eck S, Green C, Oldaker T, Stewart J, Vitaliti A and Litwin V 2019 Flow cytometry method validation protocols *Curr. Protoc. Cytom.* **87** e53
[57] Wong H N, Lewies A, Haigh M, Viljoen J M, Wentzel J F, Haynes R K and Du Plessis L H 2020 Anti-melanoma activities of artemisone and prenylated amino-artemisinins in combination with known anticancer drugs *Front. Pharmacol.* **11** 1543
[58] Balbaied T and Moore E 2020 Resazurin-based assay for quantifying living cells during alkaline phosphatase (ALP) release *Appl. Sci.* **10** 3840
[59] Wu Z, Su X, Xu Y, Kong B, Sun W and Mi S 2016 Bioprinting three-dimensional cell-laden tissue constructs with controllable degradation *Sci. Rep.* **6** 1–10
[60] Shapiro M H 2005 *Practical Flow cytometry* 4th edn (Hoboken, NJ: Wiley)
[61] Wood B, Jevremovic D, C B M, Yan M, Jacobs P and Litwin V 2013 Validation of cell-based fluorescence assays: practice guidelines from the ICSH and ICCS–part V–assay performance criteria *Cytometry* B **84** 315–23
[62] van Engeland M, Ramaekers F C, Schutte B and Reutelingsperger C P 1996 A novel assay to measure loss of plasma membrane asymmetry during apoptosis of adherent cells in culture *Cytometry* **24** 131–9
[63] Yurtdaş-Kırımlıoğlu G, Güleç K, Görgülü Ş and Kıyan H T 2022 Oseltamivir phosphate loaded pegylated-Eudragit nanoparticles for lung cancer therapy: characterization, prolonged release, cytotoxicity profile, apoptosis pathways and *in vivo* anti-angiogenic effect by using CAM assay *Microvasc. Res.* **139** 104251
[64] Ghandhariyoun N, Jaafari M R, Nikoofal-Sahlabadi S, Taghdisi S M and Moosavian S A 2020 Reducing doxorubicin resistance in breast cancer by liposomal FOXM1 aptamer: *in vitro* and *in vivo Life Sci.* **262** 118520
[65] Hsieh P-F, Jiang W-P, Basavaraj P, Huang S-Y, Ruangsai P, J-b W, Huang G-J and Huang W-C 2021 Cell suspension culture extract of *Eriobotrya japonica* attenuates growth and induces apoptosis in prostate cancer cells via targeting SREBP-1/FASN-driven metabolism and AR *Phytomedicine* **93** 153806
[66] Ilaghi M, Sharifi I, Sharififar F, Sharifi F, Oliaee R T, Babaei Z, Meimamandi M S, Keyhani A and Bamorovat M 2021 The potential role and apoptotic profile of three medicinal plant extracts on *Leishmania tropica* by MTT assay, macrophage model and flow cytometry analysis *Parasite Epidemiol. Control* **12** e00201
[67] Rebecca V W, Somasundaram R and Herlyn M 2020 Pre-clinical modeling of cutaneous melanoma *Nat. Commun.* **11** 2858
[68] Wei Q, Zhou J, An Y, Li M, Zhang J and Yang S 2023 Modification, 3D printing process and application of sodium alginate based hydrogels in soft tissue engineering: a review *Int. J. Biol. Macromol.* **232** 123450
[69] Panwar A and Tan L P 2016 Current status of bioinks for micro-extrusion-based 3D bioprinting *Molecules* **21** 685
[70] Ma X, Liu J, Zhu W, Tang M, Lawrence N, Yu C, Gou M and Chen S 2018 3D bioprinting of functional tissue models for personalized drug screening and *in vitro* disease modelling *Adv. Drug Deliv. Rev.* **132** 235–51
[71] Zhang H, Cong Y, Osi A R, Zhou Y, Huang F, Zaccaria R P, Chen J, Wang R and Fu J 2020 Direct 3D printed biomimetic scaffolds based on hydrogel microparticles for cell spheroid growth *Adv. Funct. Mater.* **30** 1910573
[72] Faulkner-Jones A, Fyfe C, Cornelissen D-J, Gardner J, King J, Courtney A and Shu W 2015 Bioprinting of human pluripotent stem cells and their directed differentiation into hepatocyte-like cells for the generation of mini-livers in 3D *Biofabrication* **7** 044102
[73] Hölzl K, Lin S, Tytgat L, Van Vlierberghe S, Gu L and Ovsianikov A 2016 Bioink properties before, during and after 3D bioprinting *Biofabrication* **8** 032002
[74] Mondal A, Gebeyehu A, Miranda M, Bahadur D, Patel N, Ramakrishnan S, Rishi A K and Singh M 2019 Characterization and printability of sodium alginate-gelatin hydrogel for bioprinting NSCLC co-culture *Sci. Rep.* **9** 1–12
[75] Calejo M T, Ilmarinen T, Skottman H and Kellomäki M 2018 Breath figures in tissue engineering and drug delivery: state-of-the-art and future perspectives *Acta Biomater.* **66** 44–66
[76] Gerecht S, Townsend S A, Pressler H, Zhu H, Nijst C L E, Bruggeman J P, Nichol J W and Langer R 2007 A porous photocurable elastomer for cell encapsulation and culture *Biomaterials* **28** 4826–35
[77] Hollister S J, Maddox R D and Taboas J M 2002 Optimal design and fabrication of scaffolds to mimic tissue properties and satisfy biological constraints *Biomaterials* **23** 4095–103
[78] Wu Z, Li Q, Xie S, Shan X and Cai Z 2020 *In vitro* and *in vivo* biocompatibility evaluation of a 3D bioprinted gelatin-sodium alginate/rat Schwann-cell scaffold *Mater. Sci. Eng.* C **109** 110530
[79] Herrera C 2019 The pre-clinical toolbox of pharmacokinetics and pharmacodynamics: *in vitro* and *ex vivo* models *Front. Pharmacol.* **10** 578
[80] Thompson M, Ellison S L and Wood R 2002 Harmonized guidelines for single-laboratory validation of methods of analysis (IUPAC Technical Report) *Pure Appl. Chem.* **74** 835–55
[81] Lee J W *et al* 2006 Fit-for-purpose method development and validation for successful biomarker measurement *Pharm. Res.* **23** 312–28
[82] Van der Walt N B, Zakeri Z and Cronjé M J 2016 The induction of apoptosis in A375 malignant melanoma cells by *Sutherlandia frutescens Evid. Based Complementary Altern. Med.* **2016** 4921067
[83] Munsky B, Neuert G and Van Oudenaarden A 2012 Using gene expression noise to understand gene regulation *Science* **336** 183–7